Research Article | Vol. 28, No. 13 / 22 June 2020 / Optics Express 19242
Optics EXPRESS

Adaptive shape control of wavefront-preserving X-ray mirrors with active cooling and heating

DANIELE COCCO,[1,2,*] COREY HARDIN,[2] DANIEL MORTON,[2] LANCE LEE,[2] MAY LING NG,[2] LIN ZHANG,[2] LAHSEN ASSOUFID,[3] WALAN GRIZOLLI,[3] XIANBO SHI,[3] DONALD A. WALKO,[3] GRANT CUTLER,[1] KENNETH A. GOLDBERG,[1] ANTOINE WOJDYLA,[1] MOURAD IDIR,[4] LEI HUANG,[4] AND GUILLAUME DOVILLAIRE[5]

[1]*Lawrence Berkeley National Laboratory, 1 Cyclotron Rd., Berkeley, CA 94720, USA*
[2]*SLAC National Accelerator Laboratory, 2575 Sand Hill Rd., Menlo Park, CA 94025, USA*
[3]*Argonne National Laboratory, 9700 S. Cass Avenue, Lemont, IL 60439, USA*
[4]*Brookhaven National Laboratory, 50 Rutherford Dr., Upton, NY 11973, USA*
[5]*Imagine Optic SA, 18, rue Charles de Gaulle, 91400 Orsay/Bordeaux, France*
[*]*dcocco@lbl.gov*

Abstract: This article describes the development and testing of a novel, water-cooled, active optic mirror system (called "REAL: Resistive Element Adjustable Length") that combines cooling with applied auxiliary heating, tailored to the spatial distribution of the thermal load generated by the incident beam. This technique is theoretically capable of sub-nanometer surface figure error control even at high power density. Tests conducted in an optical metrology laboratory and at synchrotron X-ray beamlines showed the ability to maintain the mirror profile to the level needed for the next generation storage rings and FEL mirrors.

1. Introduction

With the advent of high-repetition-rate free-electron lasers (FEL) and storage rings based on multi-bend achromat (MBA) designs, the requirement to preserve the wavefront of coherent X-ray beams is leading to increasingly stringent tolerances on mirror surface figure and alignment. In order to reach the necessary performance levels, a new generation of mirror technology has been developed along the years. This included evolutions of the original bimorph concept developed at ESRF [1,2], by using high precision multi-actuators to either compensate for the limited mirror quality [3–5] or to adapt the focal spot to the need of the experiment [6–9].

Moreover, recent progress in mirror fabrication technology [10] has made possible the realization of wavefront-preserving mirrors in diffraction-limited X-ray optical systems. Coupling such mirrors with mechanically engineered, low deformation (sub-nm) holders has provided almost perfect wavefronts for scientific applications. An example is the recent upgrade of the HXR mirrors at the Linac Coherent Light Source (LCLS) [11]. To achieve such performance, a Strehl Ratio in excess of 0.95 is required [12], meaning, in the X-ray region, the need to maintain the mirror surface within sub-nm shape errors. One significant question is whether it is possible to preserve the X-ray beam quality under medium or high heat load. For this reason, an active cooling scheme called REAL (Resistive Element Adjustable Length) has been developed and tested for implementation on the LCLS beamlines once the LCLS-II upgrade [13] is operative. The target of the cooling system described here is to correct the mid and low spatial frequency deformation associated to the thermal bump induced by beam. This approach could also be implemented on diffraction-limited storage ring (DLSR) beamlines being proposed or planned at facilities worldwide.

#394310 https://doi.org/10.1364/OE.394310
Journal © 2020 Received 2 Apr 2020; revised 13 May 2020; accepted 26 May 2020; published 15 Jun 2020

Optics EXPRESS

2. Cooling system description

The REAL cooling system has been designed and tested based on the idea described and published by some of the authors in 2015 [14] and 2016 [15]. The idea behind REAL is to compensate for the non-uniform heat load by introducing an external source of spatially adjustable heating, which will reduce thermal gradients that cause shape distortion. By applying spatially addressable heating and cooling, sub-nanometer surface figure control can be achieved under mid- to high-power X-ray beam illumination. To realize the required adaptive temperature control on the cooling of the mirror, we created a prototype, shown in Fig. 1. The cooling is achieved by copper fins (or blades) inserted in gallium-indium (GaIn) filled troughs. An array of resistive heaters is bonded to the front of each blade, at a safe distance from the gallium-indium eutectic. If the mirror would have been intended to be use on a real beamline, it would have been safer to bond the heaters on the back of the cooling pads (like shown in Fig. 1, left) to avoid that scattered light may reach directly the heaters. The electric heaters are then wired through electrical feedthroughs and remotely controlled.

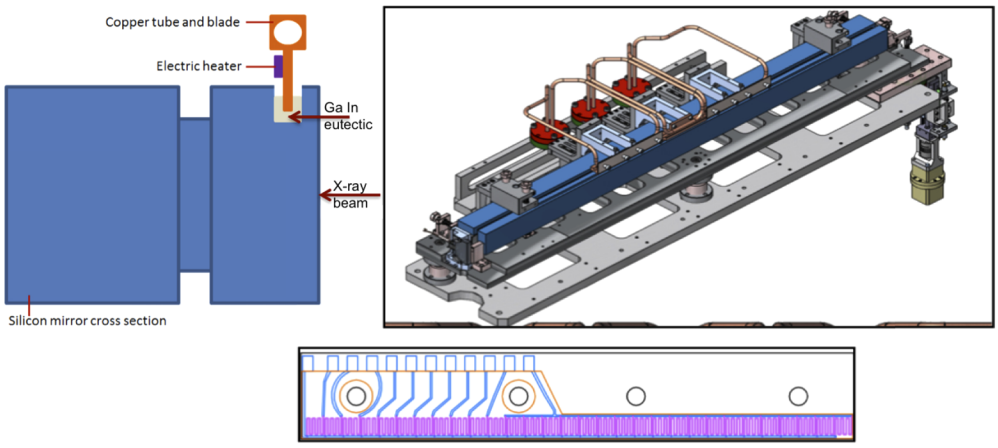

Fig. 1. Setup of the REAL cooling system used for the tests. Top Left: Cross section of the mirror showing the copper blades inserted in the GaIn eutectic filled trough and the relative heater location; Top Right: The mirror (blue) on its holder (grey) with the cooling circuit and the bender (on the right); Bottom: Drawing of the heater showing the ceramic base (white), the electric connections (blue lines) and the resistive circuits (purple).

A variable beam footprint, significantly smaller than the mirror length, induces a temperature variation in the tangential direction. The resulting thermal surface shape deformation, or 'bump,' that forms in response to the beam footprint is not cylindrical and is, therefore, difficult to correct with a mechanical bender. Since the photon beam can be variable in intensity and divergence, the heaters shown in Fig. 1 must produce a variable heated length (number and position of heaters) with adjustable heating power. The goal is to minimize the deformation of the mirror in the region illuminated by the beam to levels below the limit needed to maintain the wavefront quality. Nanometer-scale shape control is required to satisfy the Maréchal Criterion (rms wavefront error below $\lambda/14$) [16], or to meet even more stringent requirements, where required [12].

3. Tests and optimization with Infrared laser

To experimentally demonstrate the REAL principle, a 1-m-long prototype mirror, with 2-nm rms surface quality was produced by InSync, Inc. It was installed on the holder shown in Fig. 1. A model for optimizing the heater's length, based on finite-element analysis (FEA) was created

Optics EXPRESS

with the idea of refining the model after the tests. This model allowed us to define the power, length, and distribution of the heaters. The heaters were produced on a ceramic material and pressed against the cooling blades. Such heaters, even if not UHV compatible, were suitable for the metrology tests.

To simulate the thermal deformation, a class IV infrared Laser from IPG Photonics, able to deliver up to 100 W of polarized light at 1065-nm wavelength, was used. Variable absorbed power and laser beam footprint on the mirror were achieved by (1) controlling the power of the laser, (2) using cylindrical lenses to expand the beam, and (3) impinging on the silicon mirror with a grazing angle of incidence of 15°, where the absorption is maximum. The absorbed power was verified using a power meter (Ophir L50 (300)A, 400 mW-300 W, power accuracy ± 3%).

To measure the mirror surface shape, a 6-inch ZYGO DynaFiz interferometer, part of the equipment in the metrology laboratory of SLAC, was used in double-pass (or grazing incidence) mode. A thermal imaging sensor (FLIR A65) was also used to align the laser beam on the mirror and to measure the mirror temperature during the tests.

In an effort to produce a usable system, with a linear and repeatable response to the applied voltages, we developed a dedicated power supply. The heater control system designed and fabricated at SLAC consisted of a 24 V, 3.2 A, DC power supply for the Beckhoff terminals; 12 V, 10 A, DC power supply for the relays; pulse width modulation (PWM) by Beckhoff (EL2502, up to 125 kHz), and solid state relays by Crydom (DR2220D20U, up to 1 kHz). The control chassis is shown in Fig. 2, left. Each PWM control relay is connected to one resistive heater. The pulse-width inputs define the power output level of the relays that supply power to the resistive heaters. The PWMs are operated at 100 Hz, and the linearity of pulse width vs. period is preserved for the entire range of pulse width, as shown in Fig. 2 right. The linearity in the PWM ensures not only the linear thermal output from each heater but also the ability to correct small induced deformations, when power control is required in fine increments.

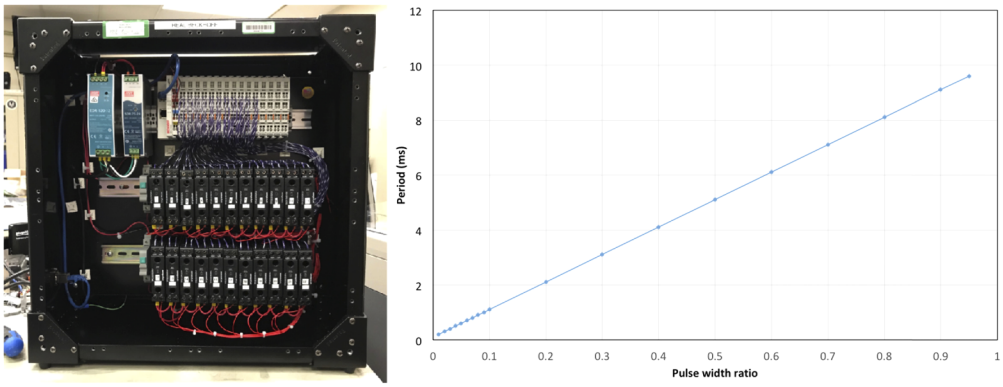

Fig. 2. Left: Picture of the control chassis hosting the heater relays. Right: Plot of the linearity of the pulse width as a function of the period the heaters are activated.

One of the first tests was the measurement of the effect of each individual heater on the mirror profile (i.e. the response function or influence function). The response of one of the 16 used heaters is shown in Fig. 3.

To make the tests meaningful, we replicated conditions similar to those expected for LCLS-II. When operating at 1 MHz, LCLS II is expected to deliver an almost monochromatic beam with up to 200 W (photon energy dependent) on the mirrors. With all the mirrors in grazing incidence, the absorbed power will never exceed 20 W and the footprints will range from 70 to 500 mm FWHM. In this particular test, we emulated the expected 130 W LCLS II beam at 1300 eV

Optics EXPRESS

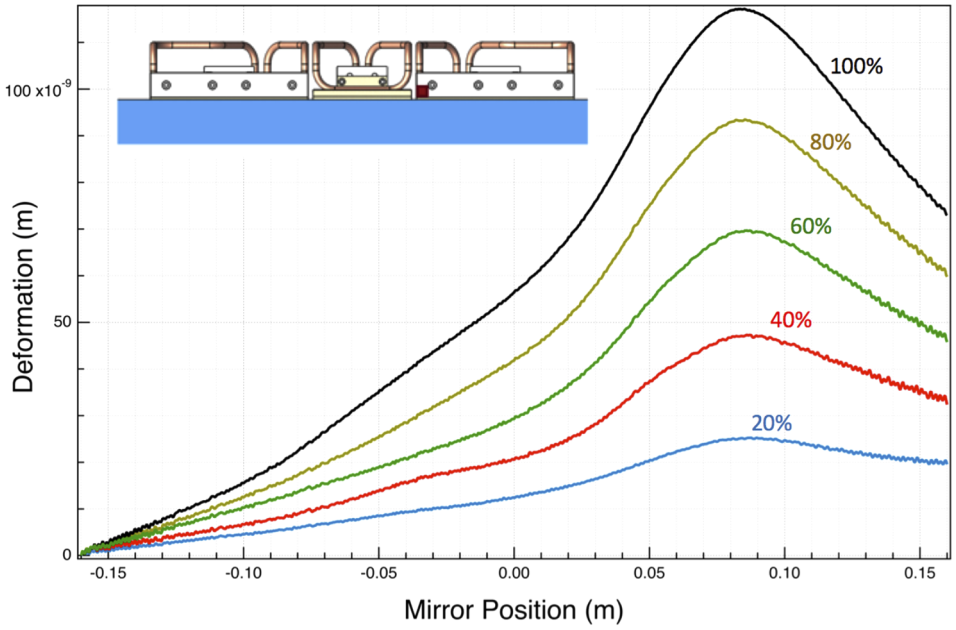

Fig. 3. Response function of one of the heaters. The heater is the closest to the center from the right side and its schematic location is shown in the inset with a red box. The deformation is measured with the interferometer, capturing only one third of the mirror length. The different curves represent the deformation induced by increasing the power of the heater from zero (not shown, but used for reference) to 100%.

photon energy. At this energy, we anticipate there will be 12 W absorbed on the first mirror, with a footprint of approximately 90 mm FWHM. The results of this test are shown in Fig. 4.

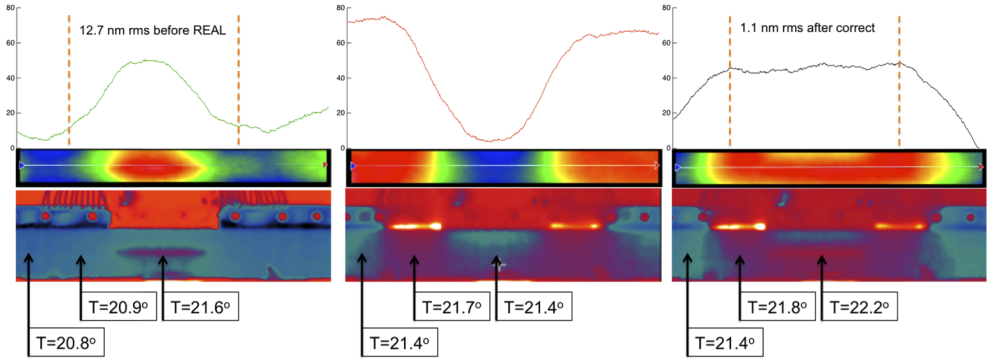

Fig. 4. Measurement of the thermally induced deformation and subsequent correction using REAL. Left: from bottom to top: Thermal image of the mirror, 2D measurement and relative profile on the center line of the mirror while irradiated by the IR laser; Center: thermal image and deformation produced by the heaters to balance the heat load bump due to the IR Laser; Right: thermal image and measurement of the mirror with the heat load corrected with the heaters. The temperature of the mirror in three characteristic points is shown.

With the conventional water-cooling scheme — water circulating in the cooling blades but electrical heater powered off — the measured residual height error was 12.9 nm rms (left of Fig. 4). To compensate for such deformation, we powered on the electrical heaters to induce

Optics EXPRESS

a correction to the shape profile shown in Fig. 4 center. Unlike the procedure adopted during the synchrotron radiation tests, described later, here the required correction was calculated by a trial and error procedure. Once the correction had been applied, the residual shape error was measured to be 1.1 nm rms in the region illuminated by the beam (Fig. 4 right).

The 1.1 nm rms residual shape error is mostly due to the mirror initial surface residual height errors measured to be 1.05 nm rms over the region of interest (between orange bars in Fig. 4). As the Fig. 4 shows, the difference arises primarily from high-spatial-frequency errors, not due to the lower-spatial-frequency shapes that we can control.

These initial tests showed that the concept of an active cooling system has the capabilities to substantially improve beamlines' wavefront preservation performance. It is worth noting that the central panel in Fig. 4 is an actual measurement, not a calculation. This can be seen as the potentiality of this system to induce a shape deformation (or correction) even in the absence of power load. Therefore, with the limit that all the thermal processes are relatively slow, the REAL system can also be considered as an adaptive optic, able to change the shape of the mirror on mid and long spatial periods if needed.

4. Synchrotron radiation tests

The mirror described above, with its cooling system and power supply, was brought to the Advanced Photon Source (APS) beamline 7-ID, for power-loading tests with hard X-ray (HXR) light. Three new heater pads with 10 individual heaters each were glued to the cooling pads. The heaters were connected to the power supply in pairs to provide a total of 15 effective heaters (Fig. 5).

The mirror deflects the beam sideways, with a fixed glancing angle of incidence of 4.2 mrad. This is intentionally above the critical angle (about 2.6 mrad) for silicon at 12 keV photon energy. In this way, the mirror absorbs more than 99% of the beam. Also in this case we replicated the conditions that are similar to those expected for LCLS-II, limiting the power absorbed by the mirror to 10 W.

Two X-ray wavefront sensors were used to test the mirror: a shearing interferometer (or Talbot wavefront sensor) and a Hartmann wavefront sensor. The Talbot wavefront sensor, developed by the APS optics group [17,18], uses a transmission phase grating (4.8-μm period, gold checkerboard) to shear the beam. The image is collected by a microscope with a LuAG(Ce) scintillator, interchangeable objective lenses for 10× and 5× magnification, and a visible-light CMOS camera with 3.1μm pixel size. Data analysis performed using a custom software (WAVEPY) [19] developed at the APS revealed the mirror surface shape under various conditions. The Hartmann sensor, developed in collaboration between Imagine Optic SA and Brookhaven National Laboratory (BNL) [8,20], has a hole-grid with 20-μm pitch, and is also equipped with a scintillator-based detection system. It provided wavefront measurements using data acquisition based on commercial software for real-time operation and advanced analysis (developed by Imagine Optic SA).

The plan for on-beamline tests was to create and measure a thermal bump arising from the HXR beam, and then correct the mirror deformation using the heaters. The first step was to characterize the effect of each heater individually, measuring the response functions to be able to predict the proper setting to compensate arbitrary deformations. For these tests, a small amount of monochromatic power was used (below 10 mW) to avoid mirror distortion. Each actuator was individually powered to 100% of its range, and the differential effect on the wavefront was measured with the wavefront sensors. Figure 6 top shows the effect of three of the 15 actuators, with their relative positions, measured by the Talbot wavefront sensor. The three actuators, numbered 5, 8 and 15 (see Fig. 5 for the equivalent location of the actuators), produced a peak-to-valley (PV) deformation on the order of 1.2–1.4 nm on the wavefront. At 4.2 mrad incidence angle, this wavefront path length change corresponds to a mirror shape

Optics EXPRESS

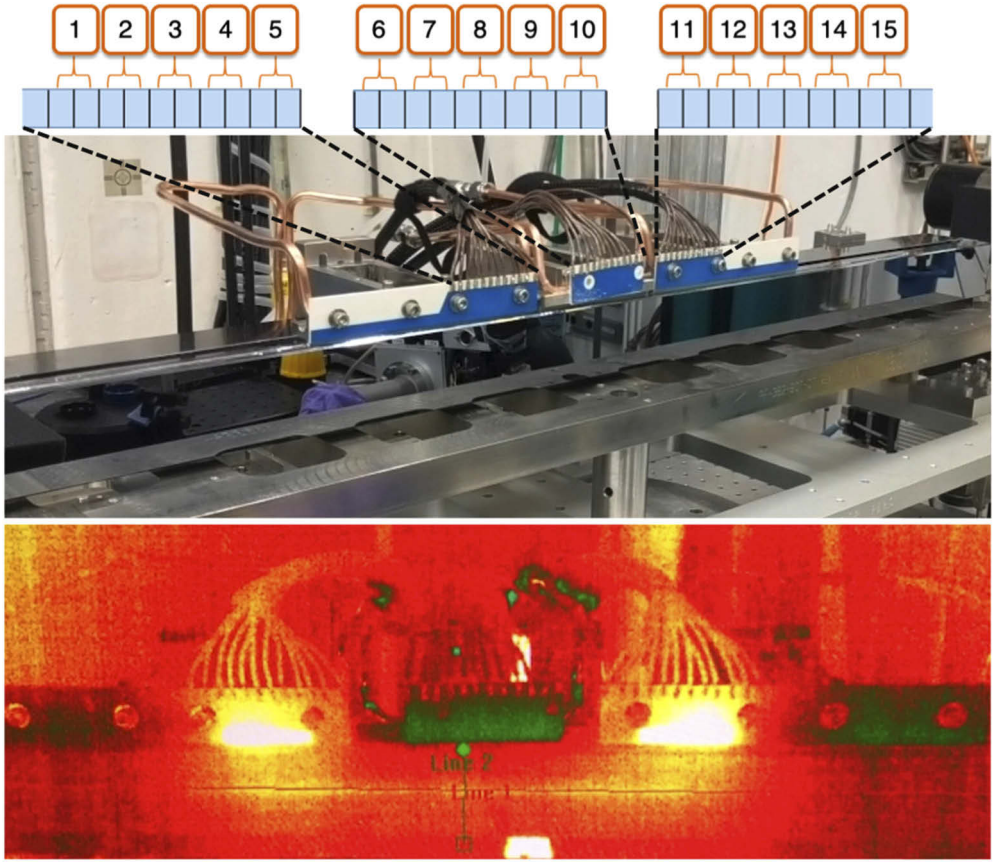

Fig. 5. The heaters nomenclature and their relative position in the REAL mirror are shown in the upper part of the figure. The mirror reflective surface is clearly visible in the central panel. Bottom: Normal incidence thermal image of the mirror showing the X-ray beam in the centre of the mirror, the heaters and the propagation of the heat through the mirror.

deformation between 140 and 160 nm. Conversion from wavefront to height error δh has been made considering that a path length variation Δs is produced by: $\Delta s = 2\,\delta h \sin\vartheta$, with ϑ being the grazing angle of incidence. All 15 actuators were characterized by both the wavefront sensors (Fig. 6 bottom). The measurements with the Talbot sensor (black curves) and with the Hartman sensor (red curves) were taken a week apart. The agreement between the two wavefront sensor results is better than 10 pm rms (1.2 nm on the mirror surface).

The temperature stabilization of the experimental hutch was not better than ±1°C. A 2°C difference is enough to produce a slight difference in radius of curvature of the measured mirror area (from 600 km to 500 km) and in the response function of the actuators (the temperature variation δT between air and heater changes). The difference between the effect of a particular heater measured with the Talbot and the Hartman wavefront sensor is reported in Fig. 7, together with the position of the heater itself. The differences have clear peaks in correspondence of the heater locations. This suggests that one of the main contributions to the measurement error is the change in the environmental conditions. If this were the only source of discrepancy between measurements taken a week apart, due to the ±1 °C temperature variation, then it would be possible to estimate the temperature stability needed. To reach stable, diffraction-limited performance, a mirror may need surface profile accuracy on the order of 0.3 nm rms or 1 nm

Optics EXPRESS

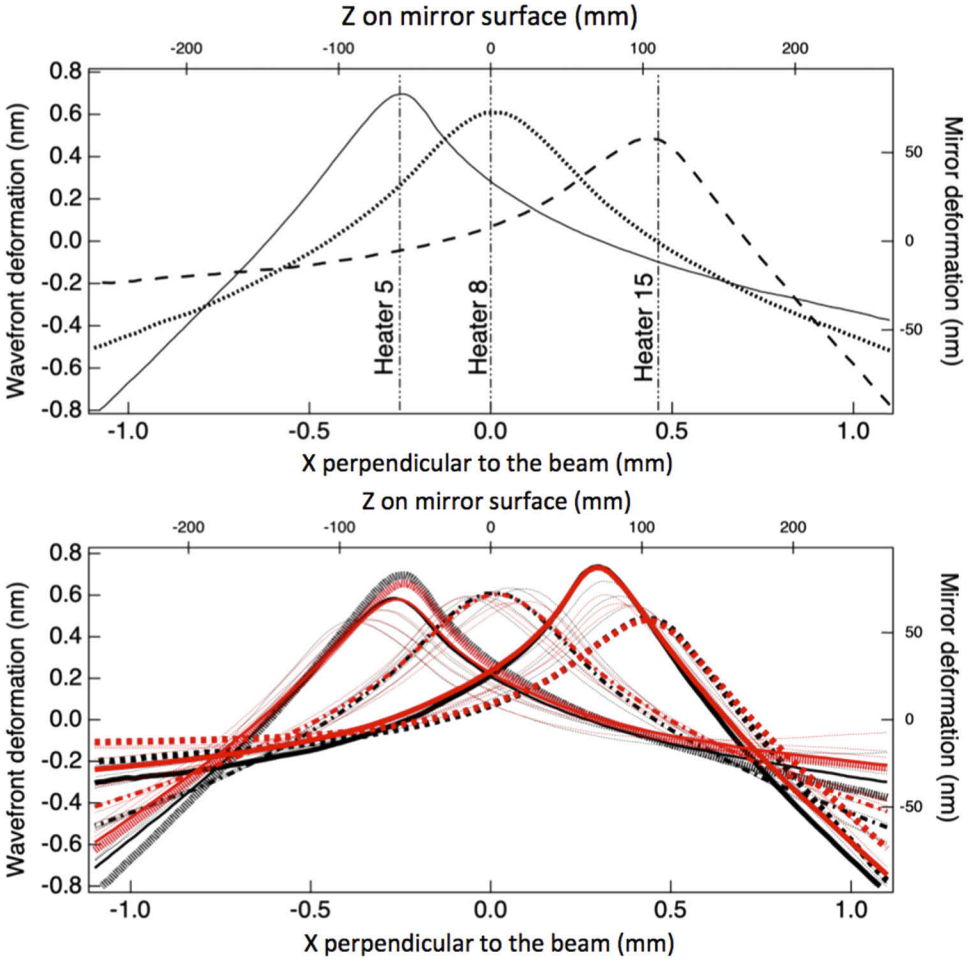

Fig. 6. Response function of the heaters. Top: Measurement with the Talbot wavefront sensor of 3 of the 15 actuators. Bottom: Measurement of all the actuators with the Talbot (black) and Hartman (red) wavefront sensor. Different line styles correspond to different actuators. The response functions are reported as a wavefront distortion (left vertical axis) and as mirror height deformation (right vertical axis). Our reference system convention is: X is horizontal, tangential to the beam, Y is vertical and Z is horizontal in the beam direction.

Optics EXPRESS

P-V (Peak to Valley). This is 4 times smaller than the observed variation. Therefore, if operating in air, the system shall be stabilized within ±0.25 °C, which is an achievable tolerance. From Fig. 6, one can also extract the level of precision at which the heater's power must be controlled. A 10 W power applied to the central heating element produces a deformation with an amplitude range of 100 nm on the mirror surface. With the target of reaching sub-nm shape control, let's say, 0.1 nm, the power shall be controlled to 10 mW precision or 1/1000 of the full range.

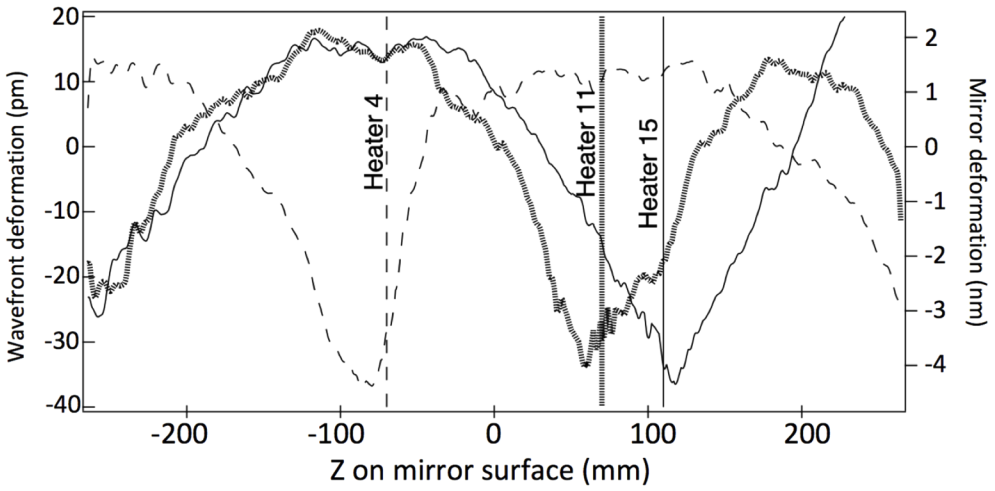

Fig. 7. Difference between the wavefront responses measured with the Talbot and the Hartman sensor for the same power applied to a given heater, but one week apart in time. The heaters presented here are number 4 (dashed thin line), number 11 (bold dotted line) and number 15 (thin full line) as labeled in Fig. 5. The position of the particular heater is also reported on the graph with a vertical line of the same pattern as the measured difference.

The measured response functions were used for the final test: increasing the power of the incident X-ray beam and compensating the thermal deformation with the heaters in a controlled way. One example of such corrections is presented here. The beam power was increased, by changing from monochromatic to white beam, to deposit roughly 10 W of 12 keV photons on the mirror on a 100 mm FWHM footprint. The induced thermal bump, shown in Fig. 8 left panels, was slightly below 400 pm P-V in the wavefront, corresponding to slightly less than 50 nm P-V on the mirror surface. This power level (10 W deposited) was selected to match the expected power absorbed by LCLS II SXR mirrors. The induced deformation by the heat-load of approximately 50 nm P-V (or 15 nm rms) on the mirror surface may look small, compared with usual thermal bump at synchrotron facilities. However, as said earlier, to preserve a diffraction-limited beam, a sub-nm rms shape error is the maximum tolerable in most situations.

Once the thermal bump generated by the beam was measured, we used calculations based on the response functions to flatten the shape in situ. The power levels needed for each actuator to correct the deformation were calculated by linear regression and applied to the mirror. Even if the measurement of the wavefront takes less than a second after applying the calculated power to the heaters, it is required to let the system stabilize thermally. For the studied mirror, environmental conditions and cooling scheme, the complete stabilization took about five minutes.

Only the central part of the induced correction affects the wavefront, since there is no beam outside the central zone. In a single step, applying power to the heaters — channel 2, 10 W; channel 10, 3.22 W; channel 12, 10 W; and channel 14, 10W (see Fig. 9 for individual and combined heaters effect) — the height deformation was reduced from 15 nm rms to 1.5 nm rms over the central line (Fig. 10), or from 115 to 16 pm rms on the 2D wavefront (see Fig. 8). The

Optics EXPRESS

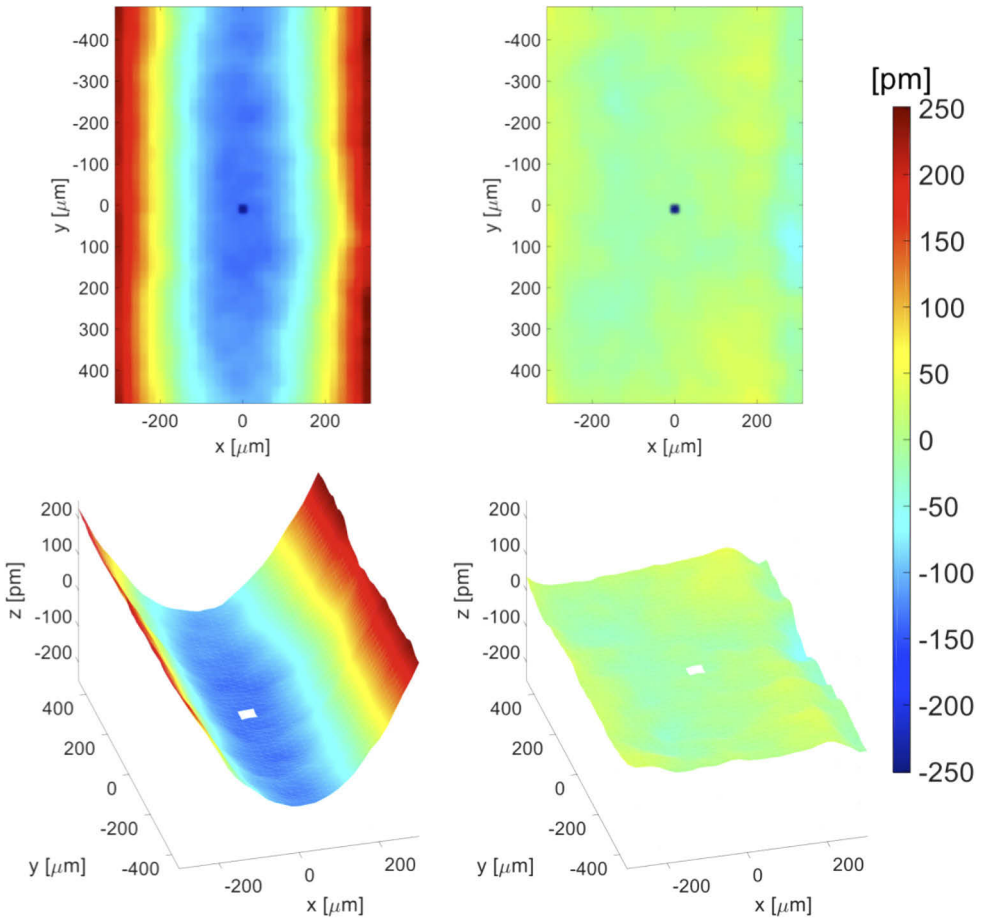

Fig. 8. In situ corrections with feedback from a Hartmann wavefront sensor. Left: before correction (114.5 pm rms, 388.9 pm P-V); Right: after correction (15.8 pm rms, 112.6 pm P-V). The scale is the same for all the figures. NOTE: X and Y are in the wavefront sensor reference system coinciding with the mirror reference system.

calculated corrected wavefront deformation and the measured one, shown in Fig. 10, are within 9 pm rms. This demonstrates the linearity of the influence function of the actuators at the sub-10 pm level, and the mirror's ability to compensate height errors by applying predictable power at the heaters

Potentially, the combination of the tools used here, i.e. non-invasive wavefront measurement and analysis in real-time, allows one to provide optimal power settings to the mirror heating channels and dynamically correct the thermal deformation (within the limit of the slowness of thermal processes). In this particular case, the fact that the tests were conducted in air with no control of the environmental conditions prevented us from exploiting the full potentiality of the correction system. In vacuum, the response function of the heaters is expected to be sharper. This will provide the possibility to correct higher spatial frequency then what can be compensated in air.

Optics EXPRESS

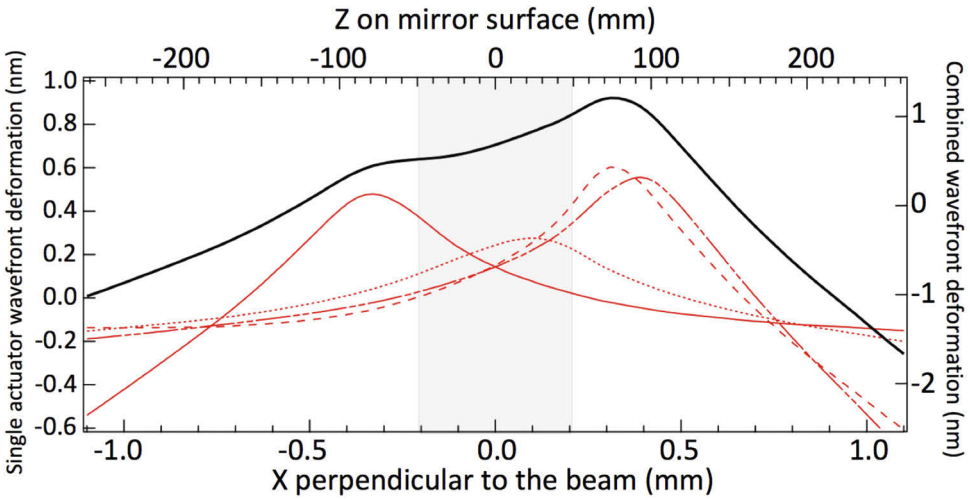

Fig. 9. The correction of the deformation shown in Fig. 8 has been obtained by combining four heaters (2, 10, 12 and 14) with different powers. The red curves represent the effect of each heater individually at the given power. The black curve represents the calculated total effect, plotted on a different scale (right scale). The grey area represents the approximate size of the photon beam.

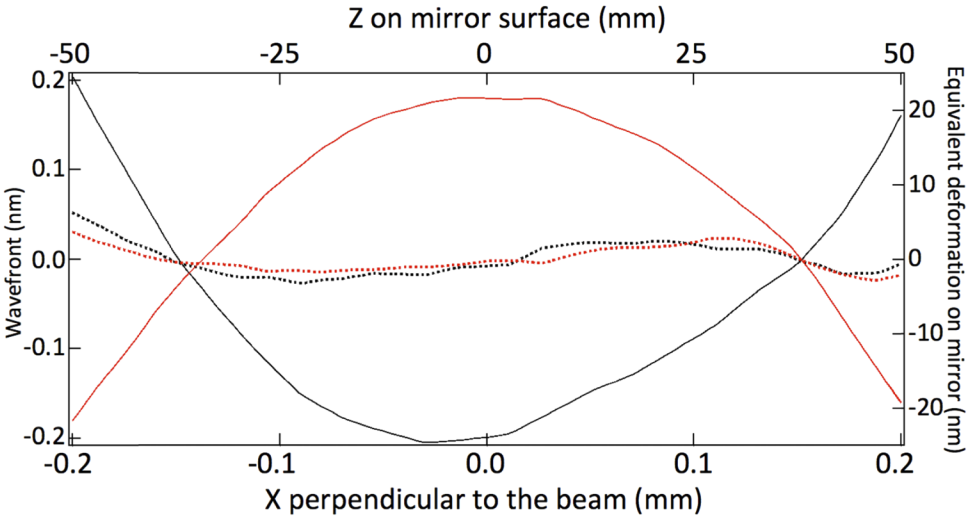

Fig. 10. Measured induced deformation (red full line) and calculated applied correction (black full line). The measured residual wavefront (or mirror surface) distortion is represented by the red dashed line. The black dashed line represents the expected wavefront (or mirror surface) profile after the correction.

5. Thermal response of the system

Since the response function is generated by heaters, an obvious side effect is the local increase of the temperature of the mirror. There is a direct correlation between mirror temperature variation, due to the heaters, and deformation. It is important to mention here that a uniform distribution of the temperature on the mirror surface is not a sign of a flattened mirror surface. This can be clearly seen in Fig. 4. Nonetheless, in principle, if the incident wavefront shape and alignment

Optics EXPRESS

were known, one could use a thermal camera alone as a non-invasive diagnostic to optimize the mirror profile. A step forward is to establish a direct correlation between the mirror induced deformation and the local mirror temperature. To do this, the five central heaters were powered in steps of 25% from zero to their maximum (10 W per heater). The time between steps was 240 s and the temperature and the wavefront were recorded every 1 second. The peak temperature was measured over the entire mirror surface, but corresponds to the area close to the heaters. The wavefront (and indirectly, mirror shape) distortion, instead, was measured along the central line of the mirror over 200 mm of length. The results are recorded in Fig. 11 and show the correlation between the peak mirror temperature and distortion of the mirror as the heater power was increased and then decreased. This measurement was made in air. During the experiment, heat transferred between the mirror and air—along with thermal transients in the mirror substrate and support—caused the apparent hysteresis in mirror distortion when decreasing heater power. The peak mirror temperature is located near the heaters, and is, therefore, less sensitive to the presence of air than the mirror distortion (see Figs. 12). We expect this hysteresis to be reduced when the system is used in vacuum.

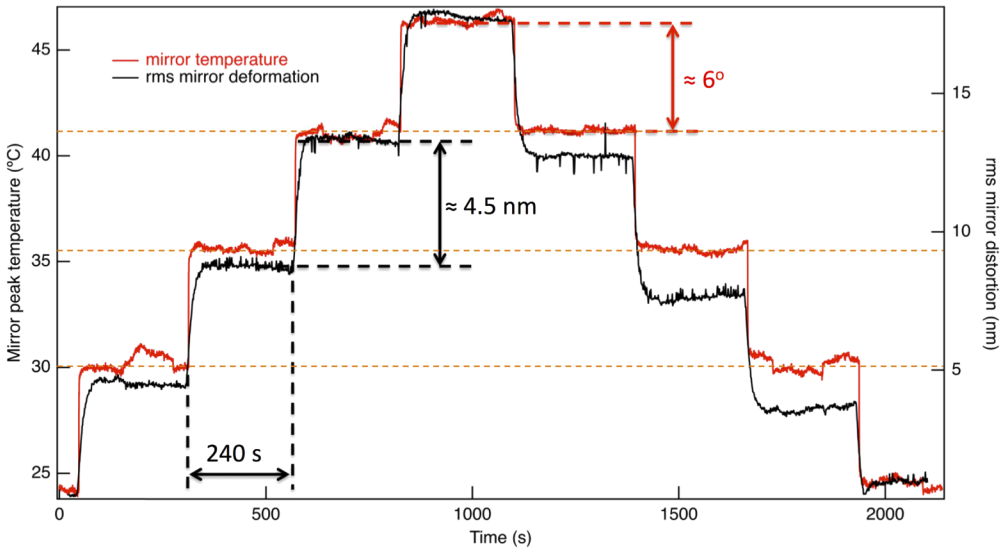

Fig. 11. Measurement of the peak mirror temperature and the rms wavefront distortion while increasing the power of the central five heaters in steps of 25% from zero to 10 W each. The black curve represents the wavefront distortion (right axis) and the red curve is the temperature (left axis). Orange horizontal lines are drawn to highlight the linearity of the thermal response of the system.

To determine the cause of this hysteresis, we used a transient thermo-elastic finite element model. The results of this model are in agreement with the measured temperature, with the caveat that the heater power in the model was approximately 10% larger than in reality. The rms distortion calculated with the finite element model is also in general agreement with measured distortion (Fig. 12), indicating that the measured temperature could be used as feedback to control the heater power. In Fig. 12, for reference only, the trend of temperature vs. deformation is reported also for the case in which the mirror is in vacuum.

Optics EXPRESS

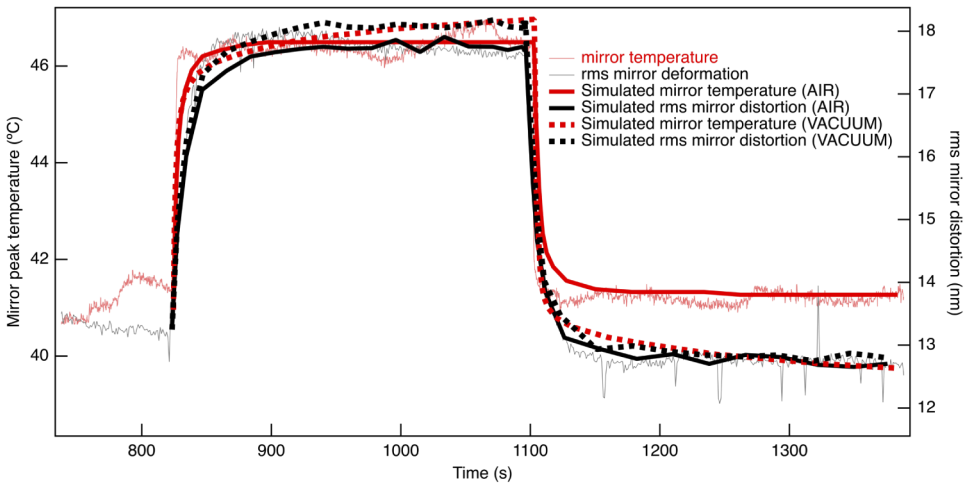

Fig. 12. Comparison between the measured temperature and mirror distortion (light red and light grey full lines, respectively) with calculated values (bold lines). One entire cycle has been calculated including heat transfer to air. The heater power has been adjusted to achieve the measured temperature variation. For reference only, the equivalent curves for a mirror in vacuum has been calculated (bold dashed lines).

6. Summary

We have demonstrated that thermally induced mirror surface height deformation, due to absorbed beam power load, can be corrected with the adoption of adaptive cooling systems, with the support of wavefront sensors to directly probe the beam quality. Applying a spatially varying heating profile reduces thermal gradients and maintains the mirror's surface quality to the desired nanometer level. In our demonstrations with absorbed power from IR and X-ray beams, corrections were made by applying heat to the cooling pads and eliminating the thermal bump. It was proven to work at the desired nm-level for absorbed powers expected at high repetition rate Free Electron Lasers (10-20 W absorbed). As a result of this study, and the experimental demonstration described here, most of the soft X-ray mirrors of the LCLS Free Electron Laser facility at SLAC, will adopt REAL as the cooling scheme.

Funding

U.S. Department of Energy (DE-AC02- 05CH11231, DE-AC02-06CH11357, DE-AC02-76SF00515, DE-AC02-98CH10886, FWP# 100318, FWP# 50513, FWP# GoldbergWPM, FWP#PS01).

Acknowledgments

We gratefully acknowledge the facilities' leadership and management for their unwavering support to this project. Special thanks is due to the APS 7-ID beamline staff for their invaluable support throughout the experiment, the SLAC technical team and the SLAC Laser Safety group, who helped in setting up the tests at the LCLS Metrology laboratory. Part of this research used resources of the Advanced Photon Source, a U.S. Department of Energy (DOE) Office of Science User Facility operated for the DOE Office of Science by Argonne National Laboratory under Contract No. DE-AC02-06CH11357.

Disclosures

The authors declare no conflicts of interest.

Optics EXPRESS

References

1. R. Signorato, O. Hignette, and J. Goulon, "Multi-segmented piezoelectric mirrors as active/adaptive optics components," J. Synchrotron Rad. **5**(3), 797–800 (1998).
2. R. Signorato and T. Ishikawa, "R&D on third generation multi-segmented piezoelectric bimorph mirror substrates at Spring-8," Nucl. Instrum. Methods Phys. Res., Sect. A **467-468**(1), 271–274 (2001).
3. L. A. Poyneer, T. McCarville, T. Pardini, D. Palmer, A. Brooks, M. J. Pivovaroff, and B. Macintosh, "Sub-nanometer flattening of 45 cm long, 45 actuator x-ray deformable mirror," Appl. Opt. **53**(16), 3404–3414 (2014).
4. L. A. Poyneer, T. Pardini, T. McCarville, D. Palmer, and A. Brooks, "Control of a 45-cm long x-ray deformable mirror with either external or internal metrology," Proc. SPIE **9208**, 92080F (2014).
5. L. A. Poyneer, N. F. Brejnholt, R. Hill, J. Jackson, L. Hagler, R. Celestre, and J. Feng, "X-ray metrology and performance of a 45-cm long x-ray deformable mirror," Rev. Sci. Instrum. **87**(5), 052003 (2016).
6. J. Nicolas, C. Ruget, J. Juanhuix, J. Benach, and S. Ferrer, "Focusing and defocusing using mechanically corrected mirrors at the MX beamline at Alba," J. Phys.: Conf. Ser. **425**(5), 052016 (2013).
7. C. Colldelram, N. González, J. González, C. Ruget, J. Juanhuix, and J. Nicolas, "Adaptive optics bender with sub-nanometer correction and stability," AIP Conf. Proc. **2054**, 060013 (2019).
8. M. Idir, P. Mercère, M. H. Modi, G. Dovillaire, X. Levecq, S. Bucourt, L. Escolano, and P. Sauvageot, "X-ray active mirror coupled with a Hartmann wavefront sensor," Nucl. Instrum. Methods Phys. Res., Sect. A **616**(2-3), 162–171 (2010).
9. C. Svetina, D. Cocco, C. Di Cicco, C. Fava, S. Gerusina, R. Gobessi, N. Mahne, C. Masciovecchio, E. Principi, L. Raimondi, L. Rumiz, R. Sergo, G. Sostero, D. Spiga, and M. Zangrando, "An active optics system for EUV/soft x-ray beam shaping," Proc. SPIE **8503**, 850302 (2012).
10. K. Yamauchi, H. Mimura, and K. Inagaki, "and Y. Mori "Figuring with subnanometer-level accuracy by numerically controlled elastic emission machining," Rev. Sci. Instrum. **73**(11), 4028–4033 (2002).
11. D. Cocco, M. Idir, D. Morton, L. Raimondi, and M. Zangrando, "Advances in X-ray Optics: from metrology characterization to wavefront sensing-based optimization of active optics," Nucl. Instrum. Methods Phys. Res., Sect. A **907**, 105–115 (2018).
12. D. Cocco, "Recent development in UV optics for ultra-short, ultra-intense coherent light sources," Photonics **2**(1), 40–49 (2015).
13. R. W. Schoenlein, A. Aquila, D. Cocco, G. L. Dakovski, D. M. Fritz, J. B. Hastings, P. A. Heimann, M. P. Minitti, T. Osipov, and W. F. Schlotter, "New Science Opportunities and Experimental Approaches Enabled by High Repetition Rate Soft X-ray Lasers," X-Ray Free Electron Lasers: Applications in Materials, Chemistry and Biology. (http://dx.doi.org/10.1039/9781782624097).
14. L. Zhang, D. Cocco, N. Kelez, D. Morton, and V. Srinivasan, "and P. Stefan "Optimizing X-ray mirror thermal performance using matched profile cooling," J. Synchrotron Radiat. **22**(5), 1170–1181 (2015).
15. C. Hardin, V. N. Srinivasan, L. Amores, N. M. Kelez, D. Morton, P. M. Stefan, J. Nicolas, L. Zhang, and D. Cocco, "Optimizing x-ray mirror thermal performance using variable length cooling for second generation FELs," Proc. SPIE **9965**, 996505 (2016).
16. A. Marechal and M. Francon, "Diffraction, structure des images; influence de la coherence de la lumiere," Masson Paris 1970.
17. W. Grizolli, X. Shi, T. Kolodziej, Y. Shvyd'ko, and L. Assoufid, "Single-grating Talbot imaging for wavefront sensing and x-ray metrology," Proc. SPIE **10385**, 1038502 (2017).
18. S. P. Kearney, L. Assoufid, W. Grizolli, T. Kolodziej, K. Lang, and A. Macrander, "Mechanical design of a compact non-invasive wavefront sensor for hard X-ray," *Proceedings of the MEDSI 2018 Conference* (pp. 394–396).
19. W. Grizolli, X. Shi, L. Assoufid, and L. G. Butler, "wavepy - Python package for x-ray grating interferometry with applications in imaging and wavefront characterization," AIP Conf. Proc. **2054**, 060017 (2019).
20. P. Mercère, P. Zeitoun, M. Idir, S. Le Pape, D. Douillet, X. Levecq, G. Dovillaire, S. Bucourt, K. A. Goldberg, P. P. Naulleau, and S. Rekawa, "Hartmann wave-front measurement at 13.4 nm with λEUV/120 accuracy," Opt. Lett. **28**(17), 1534–1536 (2003).